Title
STRAIN-RATE EFFECTS

Authors
Klahn, Dale
Mukherjee, Amiya K.
Dorn, John E.

Publication Date
1970-09-01

Presented as the keynote paper at the
2nd International Conference on the
Strength of Metals and Alloys, Asilomar,
California, Aug. 30-Sept. 4, 1970.

UCRL-20320
Preprint

c.2

STRAIN-RATE EFFECTS

Dale Klahn, Amiya K. Mukherjee, and John E. Dorn

September 1970

AEC Contract No. W-7405-eng-48

DISCLAIMER

STRAIN-RATE EFFECTS

Dale Klahn[1], Amiya K. Mukherjee[2], and John E. Dorn[3]

1. Research Metallurgist, Inorganic Materials Research Division, Lawrence Radiation Laboratory, Berkeley, California.

2. Professor of Engineering, Department of Mechanical Engineering, University of California, Davis, California.

3. Professor of Materials Science and Senior Scientist respectively of the College of Engineering and Inorganic Materials Research Division, of Lawrence Radiation Laboratory, University of California, Berkeley, California.

I. Introduction

Crystalline materials exhibit a variety of different strain-rate effects. There is no simple universally-applicable empirical law that permits the experimentally determined strain rates to be correlated with applied stresses and temperatures over wide ranges of these variables. Changes in crystal structure, grain size, composition, substructure, etc. often produce uniquely different types of plastic response. Even for the same material various types of plastic behavior are observed over special ranges of stresses and temperatures. Obviously many different deformation mechanisms contribute to the net plastic flow. It is not readily possible to satisfactorily isolate individual mechanisms for experimental examination and characterization because several mechanisms are invariably operative under any given set of conditions. For these reasons attempts to provide purely empirical correlations on strain-rate effects have not been very fruitful.

Despite its inherent complexity some success has nevertheless been achieved in rationalizing a number of important observations on strain-rate effects. Two factors have contributed to the progress that has been made: i) It is often possible to erect reasonably realistic theoretical models that permit estimates of the effects of the independent variables of stress, temperature, and substructure on the plastic strain rate appropriate for some individual mechanisms; ii) The nominal validity of such theoretical predictions can occasionally be checked by comparison with specific experimental results in the few examples and over the limited ranges of conditions where the plastic strain rates are principally responsive to that mechanism. As a result there now exists a useful, albeit somewhat incomplete, classification and detailed listing of many deformation mechanisms (1).

A brief review of several known types of deformation mechanisms will be presented in this report. Major emphasis, however, will be directed toward the synthesis and unification of strain-rate effects arising from the simultaneous operation of several mechanisms. In particular, attempts will be made to estimate theoretically dislocation velocities and plastic strain rates over wide ranges of stress and temperature. The need for improvements in theory and its extension into new and relatively unexplored regions will be pointed out in passing. Finally the theoretical deductions will be compared with experimental results on damping capacity, dislocation velocities, and plastic strain rates.

II. Types of Deformation Mechanisms. The characteristics of the several types of deformation mechanisms are revealed by the differences in the trends of the dependence of the resolved shear stress for flow, τ, on the absolute temperature, T, and the plastic shear strain rate, γ, over each of the four ranges of these variables as documented in Fig. 1 for AgMg single crystals (2-4). Whereas many other crystalline materials exhibit approximately the same general features, AgMg was selected for illustration because it provides clear delineation of each unique and distinguishable range of plastic behavior. The

designation of the various distinguishable ranges of plastic flow as due to damping, thermally-activated, athermal and diffusion-controlled mechanisms was done primarily for convenient reference. In fact all types of mechanisms are operative over all test conditions. The designated mechanisms however, will be shown to dominate over others in the prescribed ranges. It will be helpful, however, to first discuss briefly each mechanism as if it operated in complete isolation from all others and then to consider in summary the more realistic situation of simultaneous operation of several mechanisms.

A. Diffusion Controlled Mechanisms. Excluding a few rare exceptions, most metals and alloys deform by diffusion-controlled creep at low stresses and at temperatures above about one-half of their melting temperature. As shown in Fig. 1, diffusion-controlled creep at constant steady-state rates is characterized by rapidly decreasing stresses with increasing temperatures. The various diffusion-controlled creep mechanisms documented in Table I have now been identified (5).

TABLE I

Diffusion Controlled Creep Mechanisms

Subtype Mechanism	Relationship	Theoretical Justification
A. Dislocation Climb	$\frac{\dot{\epsilon}_s kT}{D_v Gb} = 2.5 \times 10^6 \, (\sigma/G)^{4.2 \text{ to } 6.7}$	[1] Good, but needs improvements
B. Climb in Dispersion strengthened alloy	$\frac{\dot{\epsilon}_s kT}{D_v Gb} = K_1 \frac{\lambda^2}{br} \, (\sigma/G)^{6.0 \text{ to } 8.0}$	[2] Needs extensive development
C. Viscous Glide	$\frac{\dot{\epsilon}_s kT}{D_s Gb} = 0.5 \, (\sigma/G)^{3.0 \text{ to } 3.5}$	[3] Good
D. Nabarro	$\frac{\dot{\epsilon}_s kT}{D_v Gb} = 5 \, (b/d)^2 \, (\sigma/G)$	[4] Excellent
E. Coble	$\frac{\dot{\epsilon}_s kT}{D_g Gb} = 50 \, (b/d)^3 \, (\sigma/G)$	[5] Excellent
F. Superplastic	$\frac{\dot{\epsilon}_s kT}{D_g Gb} = K_2 \, (b/d)^2 \, (\sigma/G)^2$	[6] Needs extensive development

$\dot{\epsilon}_s$ = Steady-state tensile creep rate

kT = Boltzmann's constant times absolute temperature

D_v = Volume diffusivity

D_s = Solute-atom interdiffusivity.

D_g = Grain boundary diffusivity

G = Shear modulus of elasticity

b = Burgers vector

d = Mean grain diameter

σ = Applied tensile stress

K_1 and K_2 = constants

λ = Spacing between particles

r = Radius of particles

Nabarro (6), Coble (7), and perhaps Superplastic (5) creep as well, are due to changes in grain shape arising directly from vacancy fluxes under chemical-potential gradients. In contrast creep by the Climb (8,9) and Viscous Glide (10) mechanisms are due to average rates of slip displacements of dislocations released by climb. At the steady state a balance must necessarily be obtained between the rate of accumulation of dislocations and their rate of removal by Climb recovery. To account for continuing steady-state creep, recovery by the Dislocation Climb mechanism must always be operative at high temperatures. For those solid-solution alloys in which strong solute-atom dislocation interactions take place (due, to Cottrell atmospheres (11), Suzuki effects (12), Fisher short-range order mechanism (13), etc.) the Viscous Glide of Dislocations becomes slower than the rates obtained exclusively by the Dislocation Climb mechanism. Although climb always occurs, the creep rate is controlled by Viscous Glide when it gives the slower rate. The total creep rate is due to the rates ascribable to either Climb or Viscous Glide, dependent on which is controlling plus the sum of rates from all remaining mechanisms. Although many mechanisms can be operable at one time, usually one exhibits the highest creep rate and therefore becomes dominant over special ranges of σ/G, b/d and T as determined also by the relative magnitudes of D_v, D_s and D_g. At temperatures somewhat below about one-half of the absolute melting temperature, however, the above mentioned diffusion-controlled creep rates become negligibly slow. It has been suggested that pipe diffusion might control creep rate at yet lower temperatures (14).

Transient creep seems to occur only when dislocation cells and entanglements are produced as a result of the initial plastic straining that takes place upon application of stress (15). During the course of transient creep such entanglements disperse and are finally replaced by the steady-state subgrain size whereupon the steady-state creep rate is obtained. In the absence of initial plastic straining, the steady-state creep rate is achieved almost immediately following stressing. Obviously Nabarro, Coble, and Superplastic Creep mechanisms do not exhibit transient stages.

B. Thermally Activated Mechanisms. Over low temperatures and for nominal rates of strain, plastic flow in crystals is usually dominated by one or more of a series of thermally-activated mechanisms. For constant plastic strain rates such thermally-activated mechanisms (vide Fig. 1) are characterized by rapidly decreasing flow stresses with increasing temperatures. The maximum temperature, T_c, over which thermally-activated mechanisms predominate depends on mechanistic details; it increases with increases in the activation energy and plastic strain rate. Two different classes of barriers have been recognized past which dislocations can be thermally activated, namely linear barriers and localized barriers. Typical examples are noted in Table II. Although the details are different, all subtype mechanisms for thermal activation of dislocations past linear barriers have in common the nucleation of slip resulting from critical bowing out of short dislocation segments as a result of thermal fluctuations in excess of the required saddle-point free energy; this is followed by a decreasing free energy as the bowed-out region spreads along the length of the previously arrested dislocation. In contrast all subtype mechanisms for motion of dislocations past localized barriers arise from individual thermal activation of separate dislocation segments that subtend each contacted obstacle whenever thermal fluctuations exceed the stress-assisted saddle-point free energy for cutting that obstacle.

The activation energies, eg. U_n or U_c of Eqs. 8 or 10, refer to the minimum work that need be done at constant temperature, pressure, and effective stress to activate dislocations over barriers. Since such energies are saddle-point free energies for activation, they necessarily obey all usual thermodynamic relationships (16-19). Several factors, however, contribute to inaccuracies in estimating such free energies. Usually the magnitude and resulting effects of inaccuracies are difficult to determine because they depend on how far the assumed model for the mechanism might deviate from physical reality. Most current calculations treat the dislocation as a string neglecting effects of orientation, radius of curvature and the influence of elastic anisotropy on the energy of the dislocation. Furthermore, as a result of the failure of Hooke's Law at high strains, estimates of interaction energies between dislocations and strain-field centers become increasingly inaccurate

TABLE II

Thermally-Activated Dislocation Mechanisms

Examples	Ref.	Prototype Model - Dislocation Velocities
A. Linear Barrier Subtypes		A. Peierls by Nucleation Rate of Kink pairs
a. Peierls	(18-25)	$v = \frac{\tau_p b^2 L \nu}{\pi^2 \Gamma_o} \exp\left\{-\frac{U_n}{kT}\right\}$ [7]
b. Pseudo-Peierls	(26)	$U_n = 2 U_k (1 - \tau^*/\tau_p)^n$ [8]
c. Cross-Slip	(27-28)	$1 \leq n \leq 2$ for usual types of Peierls hills
d. Recombination	(29)	
e. Cottrell-Lomer	(30)	
f. etc.		
B. Localized Obstacle Cutting Subtypes		B. Cutting Simple Rectangular Obstacles in Square Array
a. Repulsive dislocation trees	(11,31-35)	$v = \frac{\nu b^2}{\ell} \exp\left\{-\frac{U_c}{kT}\right\}$ [9]
b. Solute-atom stress fields	(36-41)	$U_c = \alpha \Gamma_o d - \tau^* b \ell d$ [10]
c. Guinier-Preston zones	(42-45)	
d. Radiation-damage centers	(46-50)	
e. etc.		

$\dot{\gamma} = \rho b v$ = Plastic shear strain rate [11]

ρ = Density of mobile dislocations

v = Mean velocity of mobile dislocations

τ_p = Peierls stress

ν = Debye frequency

Γ_o = Average dislocation energy per unit length

L = Distance between nodal points

ℓ = mean distance between barriers

d = width of barrier

α = Relative barrier strength ($0 \leq \alpha \leq 2$)

τ^* = Effective stress

U_n = Free energy of activation of formation of a pair of kinks

U_k = Kink energy

U_c = Free energy of activation for cutting localized barriers

at small separations where the greatest effects should be observed and the highest accuracy is usually desired. A need exists for the development of more realistic dislocation models so as to provide more accurate saddle-point estimations of free energies for activation.

Attempt frequencies for thermal activation are usually estimated in terms of the fundamental frequency of vibration of the dislocation segment that becomes activated as based on the string model. The resulting inaccuracies in the attempt frequency, however,

do not seriously affect the theoretical predictions of mean dislocation velocities. Nevertheless more sophisticated approaches to the entire problem based on detailed knowledge of partition functions would be a helpful refinement.

Eqs. 7, 8 and 11 refer to the simplest prototype model for thermal activation of dislocations past linear barriers. Other linear subtype mechanisms have many features in common with this prototype. Nevertheless each mechanism usually exhibits significant differences in the way the free-activation energy depends on the pertinent geometric dislocation details and on the effective stress. Such differences often provide a basis for possible identification of the operative rate-controlling mechanism.

The free energy of activation for cutting the different subtypes of localized obstacles also differ from one another. In general the free energy of activation can be estimated from the force-displacement (F-x) diagram (51) for cutting the obstacle as shown in Fig. 2. The saddle-point free energy of activation is given by Eq. 12.

The simplest type of force-displacement diagram is rectangular where $x_2 - x_1$ is uniformly equal to d and the maximum force is $F_m = \alpha\Gamma_o$ over distance d. This model, which has the activation energy given by Eq. 10, approximates conditions that apply when undissociated glide dislocations produce jogs upon intersecting undissociated repulsive forest dislocations. When the obstacles are arranged in a square array where $\ell = L_s$ on a side, the plastic shear strain rate is given by the Seeger (33) approximation, namely

$$\dot{\gamma} = \rho b v = \rho b \left(\frac{\lambda b}{L_s}\right) L_s \exp\left\{-\frac{1}{kT}\left(\alpha\Gamma_o d - \tau^* b L_s d\right)\right\} \qquad [13]$$

It is a simple matter to include the frequency of reversed motion of the dislocation in this formulation since the distance moved against the effective stress is L_s and therefore

$$\dot{\gamma} = \rho b^2 \nu \left[\exp\left\{-\frac{1}{kT}\left(\alpha\Gamma_o d - \tau^* b L_s d\right)\right\} - \exp\left\{-\frac{1}{kT}\left(\alpha\Gamma_o d + \tau^* b L_s^2\right)\right\}\right] \qquad [14]$$

If the obstacles are distributed more or less randomly on the slip plane, however, more obstacles will be contacted as the dislocation bows out to smaller radii of curvature, R, as the effective stress is increased. Friedel (52) has shown that the length of a dislocation subtended by randomly distributed weak obstacles is given by

$$\ell = (2 R L_s^2)^{1/3} = \left(\frac{2\Gamma_o L_s^2}{\tau^* b}\right)^{1/3} \qquad [15]$$

when there is one obstacle per area L_s^2 on the slip plane. When this value is introduced into Eqs. 9 and 10 and the frequency of reversed reactions is also considered (53)

$$v = \nu b L_s^2 \left(\frac{\tau^* b}{2\Gamma_o L_s^2}\right)^{2/3} \exp\left\{-\frac{1}{kT}\left[\alpha\Gamma_o d - 2^{1/3}\Gamma_o d\left(\frac{\tau^* L_s b}{\Gamma_o}\right)^{2/3}\right]\right\}$$

$$\left[1 - \exp\left\{-\frac{1}{kT}\left(\tau^* b L_s^2 + 2^{1/3}\Gamma_o d\left(\frac{\tau^* L_s b}{\Gamma_o}\right)^{2/3}\right)\right\}\right] \qquad [16]$$

The predicted $\tau^* - T$ relationships for (a) the Seeger approximation neglecting the reversed reaction, (b) the Seeger approximation corrected for the reversed reaction and (c) the Friedel steady-state approximation are documented in Fig. 3. Whereas the reversed reaction occurs so infrequently that its neglect is unimportant excepting for extremely small values of τ^*, the effects of τ^* on ℓ as given by the Friedel random steady-state correction, results in major changes in the $\tau^* - T$ correlations.

Identification of individual dislocation mechanisms is often made difficult as a result of simultaneous participation of several different thermally-activated mechanisms during deformation. Under two alternate sets of conditions, however, deformation rates are controlled predominantly by one mechanism: (i) When each dislocation undertakes a series of different mechanisms in sequence, the slowest becomes rate-controlling. (ii) When dislocation glide is the net result of several alternate mechanisms and the strain rate arising from one is much greater than that from all others, it becomes rate controlling. When such simplifying conditions are not realized, however, severe problems are often encountered in attempts to establish useful theoretical formulations for rationalizing strain-rate effects. Although other pertinent examples could be added to this list, the following are illustrative of types of problems that now deserve more detailed attention:

a. Statistical analyses for distributions of localized strain centers of variable strengths, such as encountered in solid solutions or radiation damage, on the strain-rate effects.

b. Modifications of strain-rate effects for the Peierls mechanism as a result of solid-solution alloying.

c. Conditions that prevail when both thermally-activated cross slip as well as cutting localized strain centers prevail.

C. Athermal Deformation Mechanisms. As illustrated in Table III, athermal dislocation mechanisms fall into two general classes.

TABLE III

Athermal Dislocation Mechanisms

Subtype	Example	Ref.	Athermal Stress	
a. Inherent	a. Fisher's SRO	(13)	$\tau_{1A} = CN_a N_b \alpha_c \varepsilon_B$	[17]
	b. Cutting APBs	(54)	$\tau_{2A} = \frac{\gamma_A}{\delta'}\left(1 - \frac{6b}{\delta'}\right)$	[18]
b. Conditional	a. Cutting Attractive Junctions	(55-58)	$\tau_{3A} = \beta_s Gb\sqrt{\rho}$	[19]
	b. Long-Range Back Stresses	(59-61)	$\tau_{4A} = \beta Gb\sqrt{\rho}$	[20]

$\tau_A = \sum_j \tau_{jA}$ [21] Total operative athermal stress level

$C = 16/\sqrt{6}$ for bcc alloys

N_a, N_b = Atomic fractions of a and b atoms

α_c = Cowley's degree of short-range order

$\varepsilon_B = \varepsilon_{AB} - (\varepsilon_{AA} + \varepsilon_{BB})/2$ = Bond energy

γ_A = Antiphase boundary energy/cm^2

δ' = Antiphase domain diameter

$\beta_s \approx \beta \approx 1/5$

Inherently athermal mechanisms are characterized by a continuously increasing free energy as a dislocation is forced through the crystal. In this case no saddle-point free energy is ever attained and consequently the process cannot be facilitated by thermal fluctuations; dislocations can only be moved mechanically under the athermal stress level suggested in Table III. Conditionally athermal mechanisms are similar to thermally-activated mechanisms insofar as the free energy reaches some maximum value upon displacement of the dislocation; they differ from common thermally-activated mechanisms either because the saddle-point free energy is vastly greater than kT or because long segments of dislocations must be moved relatively far distances before the saddle-point free energy is reached. In either event

sufficiently energetic thermal fluctuations will be so infrequent as to have a negligible effect on the strain rate. The stresses necessary to overcome the inherently athermal dislocation mechanisms are practically independent of the temperature especially in the interesting range of low temperature where frozen-in, short-range and long-range order prevail. The athermal stress levels that depend on mutual interaction of dislocations, such as τ_{3A} and τ_{4A}, decrease only slightly with increasing temperature according to $\tau_{jA} = \tau_{jAo} G/G_o$ [22] where the subscript zero refers to the absolute zero of temperature.

The estimate of $\beta \simeq 1/5$ in Eq. 20 is generally verified experimentally (5, 62). But the fact that the estimate for β_s of Eq. 19 is about the same prompts the important question as to whether or not both mechanisms are equally important in accounting for strain hardening. The value of Saada's estimate $\beta_s \simeq 1/5$ was deduced as a simple average of the cutting stress over the expected range of strengths for attractive junctions, neglecting the often pronounced reductions that are expected as a result of the more or less random distribution of attractive junctions on the slip plane. As suggested by the somewhat simpler cases studied by Foreman and Makin (63), the value for β_s is expected to be considerably less than that of 1/5 when randomness is invoked. It therefore appears that the major factor responsible for strain hardening arises essentially from effects of long-range book stresses rather than the formation of attractive junctions. Many other factors, however, also contribute to strain hardening.

D. Viscous Drag Mechanisms. Although viscous drag mechanisms are operative whenever dislocations move, they become rate-controlling, as shown in Fig. 1, when the stresses are sufficiently high to mechanically force dislocations past all barriers without awaiting aid from thermal fluctuations. The stress level at which damping mechanisms first become rate controlling are dependent on the athermal stress, the total energy for thermal activation and the temperature. Experimental data, however, suggests that in most metals and alloys this usually happens as soon as the plastic shear strain rate first exceeds a value of about 3×10^3 per second or when the mean dislocation velocity is above about 10^3 cm/sec.

All viscous drag mechanisms considered here are Newtonian and consequently the drag force acting on a unit length of a moving dislocation is given by

$$\tau_B b = Bv \qquad [23]$$

where $\tau_B b$ is the drag force and B is the net drag coefficient. As the dislocation velocity approaches that for sound waves, relativistic factors serve to modify some of the non-relativistic drag coefficients and the simple linear relationship between stress and dislocation velocity of Eq. 23 no longer applies. Partial progress (64-69) has been made theoretically in defining some of the conditions that are to be encountered when dislocations enter the relativistic range with velocities approaching that of sound and when dislocations become supersonic. Many theoretical details encountered at high dislocation velocities however, need yet to be explored, especially e.g., the form taken by Eq. 23. Furthermore there appear to be no reliable and analysable experimental data for attenuation, dislocation velocities, or plastic strain rates for cases where the dislocation velocities begin to approach those for sound waves.

Theoretical estimates for the coefficients B_i, appropriate for various dislocation mechanisms limited to conditions where $v \lesssim c/e$ where c is the velocity of sound, are documented in Table IV.

Each of the five dislocation-drag mechanisms documented in Table IV are different. The net drag coefficient, B, is thus the sum of those for each independent mechanism. Contributions to B from thermoelastic damping, however, are almost always negligible. In general the contribution to B arising from phonon scattering is about one order of magnitude less than that from phonon viscosity. Electron scattering and electron viscosity mechanisms are only operative in electronic conductors.

TABLE IV

Dislocation-Drag Mechanisms

Subtype	Ref.	Origin and Comments
A. Thermoelastic $B_1 = \frac{Eb}{13c}$ . . . [24]	(69-71)	Energy loss due to irreversible heat flow from the compressional to dilatational side of moving edge dislocation; Contribution about zero for a screw dislocation. Effect of temperature as on E.
B. Phonon Scattering Liebfried $B_2 = \frac{Eb}{10c}$ . . . [25] Eshelby Lothe $B_2 = \frac{Eb}{12c}$, in core	(72-74)	Drag results from the net difference in the momentum of scattered phonons from the front and back of moving dislocation. Drag coefficient increases only slightly with increasing T above Debye temperature as dictated by E.
C. Electron Scattering $B_3 = \frac{3}{128}\frac{2\pi}{h}\left(\frac{B_c}{E_f}\right)^2\left(\frac{\rho_m}{K_f}\right)K_f^2 h^2 N_e b^2$ $\approx \frac{1}{16}\frac{B_c^2}{h^3} m_e^2 \rho_m b^2$ . . . [26]	(75,76)	Scattering of electrons in electronic conductors by the stress field of moving dislocation by mechanism analogous to phonon scattering. Drag coefficient is independent of temperature.
D. Phonon Viscosity $B_4 = \frac{b^2\eta_p}{8\pi a_o^2}$ . . . [27] $\eta_p = \frac{DEK_o}{C_v c^2}$	(77-80)	Difference in the shear strain rates as the dislocation moves causing a separation of the vibration frequencies of the different phonon modes. Energy loss is due to dissipation of heat from the phonons having higher temperature to the cooler ones. Slightly different for edge and screw components. Drag coefficient vanishes at T=0 and increases up to Debye temperature and thereafter increases only slightly with increasing temperature.
E. Electron Viscosity $B_5 = \frac{b^2\eta_e}{8\pi a_o^2}$ . . . [28] $\eta_e = \frac{9 \times 10^{11} h^2 (3\pi^2 N_e)^{2/3}}{5\, e^2 \rho_e (2\pi)^2}$	(81,82)	Momentum changes in electronic conductors due to strain field of moving dislocation and transfer of momentum from electrons to phonons, resulting in heat dissipation. Drag coefficient is strongly temperature dependent and follows the temperature dependence of ρ_e^{-1}.

a_o = Cut-off radius of dislocation core

B_i = Drag coefficients

B_c = Electron-phonon coupling constant

C_v = Specific heat per unit volume

D = Nonlinearity constant, can be calculated from third order elastic constants

$e = 4.8 \times 10^{-10}$ esu = Electronic change

E = Thermal energy density

E_f = Fermi energy

h = Planck's constant

K_p = Thermal conductivity due to phonons.

K_f = Wave vector of an electron at the Fermi level

N_e = Number of free electrons per cc

m_e = Mass of an electron

ρ_e = Electrical resistivity ohm-cms

η_p = Phonon viscosity

q_m = Typical Fourier component of the strain field associated with the dislocation

η_e = Electron viscosity

Although the operation of the listed mechanisms is well established, questions have arisen regarding (a) how realistic the assumed models for each mechanism might be and (b) how accurately the analyses based on each model might have been carried out. The questions are particularly pertinent for the mechanisms that involve electrons. For example Bommel and Tittman (83) have questioned whether the electron viscosity model of Mason (81,82) is applicable under usual experimental conditions- and Mason's reply (84) suggest that he considered it to be valid provided the dislocation velocities remained substantially less than the speed of sound.

In addition to theoretical questions there appears to be unresolved differences in some of the experimental results. Some attenuation measurements (85) for Al, Cu, and Pb show a strong temperature dependence of B at low temperatures, which seems to be in accord with Mason's electron viscosity model. On the other hand, recent measurements on Pb (86) an Al (87), which show that B is essentially independent of temperature at low temperatures, tend to support the electron scattering model. Such experimental inconsistencies must be resolved before more light can be shed on these issues.

E. Recapitulation with Summary on Major Classes of Deformation Mechanisms. Usually several subtypes in each of the four major classes of deformation mechanisms operate simultaneously so as to co-operatively determine by their mutual interactions the net effect of that major class on the strain rate. Methods for estimating such combined effects for certain simple cases have already been suggested for the major deformation mechanisms of diffusion-controlled creep, athermal processes, and dislocation-drag phenomenon. The net effects arising from the simultaneous operation of several thermally-activated mechanisms, however, is usually quite complicated due to intimate interactions between them. More complete examination of combined effects of simultaneous operation of several individual thermally-activated mechanisms need be made.

All four major types of mechanisms are operative at any one time. Over limited ranges of conditions, however, one of these mechanisms becomes predominant. Nevertheless the effects of the remaining mechanisms are detectable. A principal objective of this report concerns rationalization of strain-rate effects when several major deformation mechanisms are simultaneously operative. For the remainder of this paper the conditions will be limited to those where diffusion-controlled creep is negligibly slow. Consequently only those strain-rate effects ascribable to combinations of athermal, thermally-activated, and dislocation-drag mechanisms will be considered. For clear emphasis of mutual interactions between these major classes of mechanisms, they will be considered first in combinations of pairs. Finally the strain-rate effects for simultaneous operation of all three major classes of mechanisms will be illustrated.

III. Combined Effects of Athermal and Thermally-Activated Mechanisms. At low temperatures and not too high strain rates, plastic deformation is determined principally by combined results of athermal and thermally-activated mechanisms. It has been common practice to assume that the athermal and effective stresses superimpose to give the applied stress, τ, according to

$$\tau = \tau^* + \tau_{jA} \qquad [29]$$

resulting in the combined effects as shown graphically in Fig. 4A. Whereas the simple super-position principle is patently valid when the athermal stresses result exclusively from short-range order or antiphase boundary effects, it fails when the athermal stresses arise either from breaking attractive junctions or from surmounting long range stress fields.

The general kind of correlation that is expected when the athermal stress arises exclusively from breaking attractive junctions can be approximated by neglecting all geometric statistical factors and assuming that attractive junctions and repulsive trees, having strengths α_A and α respectively, are laid down in a regular square array of side L_s, on the slip plane. When, under the applied stress τ, dislocation segments are thermally activated past repulsive trees, the force on the attractive junctions will increase and break them athermally. The usual analysis for simple thermally activated mechanisms applied to this model gives the relationship

$$\dot{\gamma} = \rho b^2 \nu \exp\left\{-\frac{1}{kT}(\alpha\Gamma_0 d - \tau L_s b d)\right\} \qquad [30]$$

$$\tau_{3A} = \frac{\alpha_A \Gamma_0}{2L_s b} \qquad [31]$$

As shown graphically by the lower solid lines in Fig. 4B the interpretation here is uniquely different from that presented in Fig. 4A. The critical temperature, T_c, shown in Fig. 4B, is given by

$$\alpha\Gamma_0 d = kT_c \ln \frac{\rho b^2 \nu}{\dot{\gamma}} \qquad [32]$$

and therefore it is also independent of L_s just as it is when Eq. 29 is assumed.

Over Stage II for strain hardening in fcc metals the Cottrell-Stokes (88) ratio τ_{T1}/τ_{T2} of the flow stress at T_1 to that at T_2 is known to be insensitive to the strain-hardened state. In contrast the model outlined above, based on the hypothesis that the athermal stress arises completely from attractive junctions, makes predictions at variance with these experimental facts. This is most readily seen by assuming that L_s is decreased by strain hardening to give the upper curves of Fig. 4B. Consequently according to this model the Cottrell-Stokes ratio is not constant but should increase with strain hardening. This deviation from experimental fact suggests that attractive junctions do not generally play a significant role in strain hardening; this deduction coincides with conclusions previously presented in Section II, that the random distribution of attractive junctions, on the slip plane should give smaller values of β_s than estimated by Saada. The alternate hypothesis that athermal stresses associated with dislocation mechanisms are principally due to their long-range internal stress fields, τ_i, rather than attractive junctions appears to have more justification. The detailed and specific distribution of such internal stresses is not yet well known except for the requirement that $\int\int \tau_i \, dxdz = 0$ over the x-z slip plane. If adjacent segments of a dislocation line were to lie in regions where the sign of τ_i alternated from plus to minus, the average force on the total dislocation would arise almost exclusively from the externally applied stress, since those forces due to the oscillating internal stress fields and the oscillating dislocation curvatures would negate each other. Under such circumstances the internal stress field would exert practically no effect on the dislocation velocity. It is more likely, however, that as a result of their mutual interactions long segments of dislocations having the same Burgers vector will be forced to lie parallel to one another and therefore parallel to the internal stress fields they generate. Consequently when the dislocation is taken to be parallel to the z-axis, τ_i will vary only with x. Although this variation is expected to be quite random in wave length and amplitude, the general effect can be approximated by taking the major term of a Fourier representation of τ_i namely

$$\tau_i = \tau_{4A} \sin \frac{2\pi x}{\lambda} \qquad [33]$$

as shown in Fig. 5. A sinusoidal internal stress field variation has been shown by Mix, Coghlan and Barrett (89) to be an accurate representation of the stresses arising from dislocations in square arrays. Other analytical treatments of dislocations moving in periodic stress fields have been formulated by Chen, Gilman and Head (90), Evans, Bailey and Flanagan (91), Arsenault and Li (92), Adams (93), Li (94) and Argon (95). Obviously the suggestion contained in Eq. 29 that τ_{iA} and τ^* superimpose to give τ is inaccurate for such models of the origin of athermal stresses.

As will be discussed more fully later, the inertia of dislocations is so small that they respond extremely rapidly to commonly encountered changes in force acting on them. Consequently their equation of motion can be accurately represented by

$$\frac{dx}{dt} = v \qquad [34]$$

where $v = v\{x\}$ is the instantaneous velocity at x due to the operative mechanism. To illustrate the issues involved, Eq. 34 will be applied to the simple Seeger approximation for intersection of dislocations represented by Eqs. 9 and 10. Then the average time, t, that a dislocation will take to traverse a wave length λ is given by

$$\bar{t} = \int_0^{\bar{t}} dt = \int_0^{\lambda} \frac{dx}{v} = \frac{\displaystyle\int_0^{\lambda} \exp\left\{\frac{\tau_{4A} L_s b d}{kT} \sin\frac{2\pi x}{\lambda}\right\} dx}{\nu b \exp\left\{-\frac{1}{kT}\left(\alpha\Gamma_o d - \tau L_s b d\right)\right\}} \qquad [35]$$

and the mean velocity reduce to

$$\bar{v} = \frac{\lambda}{\bar{t}} = \nu b \exp\left\{-\frac{1}{kT}\left[\alpha\Gamma_o d - (\tau - \psi\tau_{4A}) L_s b d\right]\right\} \qquad [36]$$

where ψ, obtained by analytical integration of Eq. 35, is a function of the dimensionless quantity $\phi = \tau_{4A} L_s b d/kT$ as shown in Fig. 6.

The corresponding τ - T curve for a constant strain rate is

$$\tau = \psi\tau_{4A} + \frac{\alpha\Gamma_o}{L_s b} - \frac{kT}{L_s b d} \ln \frac{\alpha b^2 \nu}{\dot{\gamma}} \qquad [37]$$

as shown in Fig. 4C. For this model the appropriate equation for superposition of stress is given by $\tau = \tau^* + \psi\tau_{4A}$ [38] in lieu of Eq. 29. Furthermore Eq. 37 is not at variance with the constancy of the Cottrell-Stokes ratio for fcc metals over Stage II since this experimental fact merely confirms that τ_{4A} varies with strain-hardening as $1/L_s$ in consonance with all other terms of Eq. 37 that determine τ. The reinterpretation of the superposition condition suggested by this model is by no means trivial especially for high values of τ_{4A} and particularly when detailed analyses of all factors including the value of the pre-exponential term in the strain-rate expression is desired.

Although the details are slightly more complicated, the same general procedure of accounting for the effects of long-range internal stresses can be applied to the expression for v when it is corrected for randomness of localized barriers as given by Eq. 16. The development of analytical procedures for accounting for effects of long-range back stresses

in cases where the barriers are linear, however, have not yet been fully explored. If, the critical condition for thermal activation of the Peierls mechanism always remains the frequency of nucleation of kink pairs, the general procedures that were described previously remain applicable.

IV. Combined Effects of Thermally-Activated and Dislocation-Drag Mechanisms. In terms of Fig. 1 it might appear that a sharp demarkation exists between the higher strain-rate region where the deformation rates depend principally on drag mechanisms and the slightly lower strain-rate regions where thermally-activated mechanisms appear to be rate controlling. Since both types of mechanisms are simultaneously operative everywhere it becomes important to ascertain what mutual interactions take place as a result of their simultaneous operation.

As shown by Frank (96), the energy Γ of a straight screw dislocation moving with a constant velocity is

$$\Gamma = \Gamma_o \{1 - (v/c)^2\}^{-1/2} \simeq \Gamma_o + \frac{1}{2}\frac{\Gamma_o}{c^2} v^2 + \text{---} \qquad [39]$$

where Γ_o is its rest energy and c is the velocity of a shear wave. For the cases considered here where $v/c < 1/3$, the first term of the Taylor's expansion is the potential energy the second term is the kinetic energy per unit length of dislocation and all higher order terms are negligible. Consequently the effective mass per unit length of a dislocation is given by the small value Γ_o/c^2 and the equation of motion of a straight screw dislocation becomes

$$\tau^* b - Bv = \Gamma_o/c^2 \frac{dv}{dt} \qquad [40]$$

Taking the boundary conditions as $v = o$ at $t = o$ gives

$$v = \frac{\tau^* b}{B}\left[1 - \exp\left\{-\frac{Bc^2 t}{\Gamma_o}\right\}\right] \qquad [41]$$

For the usual values of $B \simeq 3\times10^{-4}$, $\Gamma_o \simeq 10^{-5}$, $c^2 \simeq 10^{10}$, in c.g.s units, the dislocation velocity acquires 95% of its steady-state velocity of $\tau^* b/B$ in the extremely short time of about 10^{-11} sec. Somewhat similar expressions apply for edge dislocations. Consequently in most cases, even including many dynamic experiments, dislocations acquire their steady-state velocities almost instantaneously. The conclusion is equally valid when thermally-activated mechanisms are also operative in addition to dislocation-drag mechanisms.

The general trends for strain-rate phenomenon arising from the combined effects of dislocation-drag and thermally-activated mechanisms are expected to be somewhat similar whether the thermally-activated mechanism is that for activation of dislocations past localized obstacles or linear barriers. Analyses based on linear barriers, however, are complicated and consequently the combined effects of the two major types of mechanisms will be developed here only for the simplest representative example of thermal activation over a square array of localized obstacles as illustrated in Fig. 7. Under the action of a stress a dislocation (i) contacts localized obstacles at $t = o$, (ii) bows out, (iii) cuts the obstacle when $t = t_1$, and (iv) continues in pure-drag flight until it again contacts the next set of obstacles when $t = t_3$. The pure-drag-flight interval is $t_2 = t_3 - t_1$. Consequently the mean dislocation velocity is $\bar{v} = L_s/(t_1 + t_2)$. [42]
The dynamic equilibrium equation applicable to the bowing out period is

$$\tau^* b - Bv = \Gamma_o/R \quad \text{for} \quad o \le t \le t_1 \qquad [43]$$

where v is the dislocation velocity normal to its segment and R is its local radius of curvature. An alternate procedure to that proposed by Frost and Ashby (97) for calculating

t_1 will be adopted here. When the slopes of the dislocation lines are small relative to unity, Eq. 43 reduces to

$$\tau^* b - B \frac{\partial y}{\partial t} = - \frac{\partial^2 y}{\partial x^2} \qquad [44]$$

For the operative boundary conditions of $y = 0$ at $t = 0$, and $y = 0$ at $x = \pm L_s/2$ for all t, the solution (98) to Eq. 44 is

$$y = \frac{\tau^* b L_s^2}{8\Gamma_o} \left[1 - \left(\frac{2x}{L_s}\right)^2 - \frac{32}{\pi^3} \sum_{m=o}^{\infty} \frac{(-1)^m}{(2m+1)^3} \cos \frac{(2m+1)\,\pi x}{L_s} \exp \left\{ - \frac{\Gamma_o (2m+1)^2 \pi^2 t}{B L_s^2} \right\} \right] \qquad [45]$$

The time t_1 is that for which the probability for a successful thermal fluctuation for cutting a localized obstacle is unity. It can be evaluated in terms of the frequency ν for cutting obstacles of strength α for a square array, namely

$$\nu \frac{\nu b}{L_s} \exp \left\{ - \frac{1}{kT} (\alpha \Gamma_o d - 2\Gamma_o d \sin \theta) \right\} = \frac{\nu b}{L_s} \exp \left\{ - \frac{2\Gamma_o d}{kT} (\sin \theta_c - \sin \theta) \right\} \qquad [46]$$

where θ is defined in Fig. 7 and $2\,\Gamma_o \sin \theta$ is the time-dependent force acting on the obstacle. Also for convenience α is replaced by $2 \sin \theta_c$ where θ_c refers to the value of θ at which obstacles will be cut athermally. Consequently t_1 is determined by

$$1 = \int_o^{t_1} \frac{\nu b}{L_s} \exp \left\{ - \frac{2\Gamma_o d}{kT} (\sin \theta_c - \sin \theta) \right\} dt \qquad [47]$$

$$\sin \theta = \left\{ \frac{dy}{dx} \Big/ \sqrt{1 + \left(\frac{dy}{dx}\right)^2} \right\} x = - \frac{L_s}{2} \qquad [48]$$

as deduced from Eq. 45.

The assumption of small slopes is reasonably accurate for weak obstacles, e.g. those for which $\sin \theta_c \leq 0.2$. For stronger obstacles a valid alternate approximation, to be detailed in a future paper, can be employed. Since the inertia of dislocations is small, t_2 was quite accurately approximated by

$$t_2 = (L_s - \bar{y})/v = B\,(L_s - \bar{y})/\tau^* b \qquad [49]$$

where $\bar{y}$ is the average value of y when $t = t_1$ and is obtained analytically from Eq. 45.

Fig. 8 illustrates, in dimensionless terms, how the average dislocation velocity varies with effective stress for a series of temperatures. In this representation B was taken to be independent of the temperature. Consequently the predicted variations of $\bar{v}$ with T reflects the effect of temperature on the frequency for thermal activation. As the temperature is increased the delay time for successful thermal fluctuations is being continually reduced, and consequently v approaches ever more closely the value predicted by the dislocations-drag limit. The circles on each different temperature curve refer to the condition for which $t_1 = t_2$. Consequently points on each line below each circle refer increasingly to conditions where $\bar{v}$ is evermore dependent on successful thermal fluctuations whereas points above each circle refer to conditions where $\bar{v}$ is evermore dependent only on dislocation-drag mechanisms. The effects of localized barriers in reducing $\bar{v}$ are noted to persist for stresses above $\tau^*/\tau_c = 1$ and the effect of dislocation-drag mechanisms

remain significant even for stresses somewhat below $\tau^*/\tau_c = 1$.

An alternate representation of Fig. 8 is shown in Fig. 9 which parallels the experimental trends recorded in Fig. 1. The broken line constitutes the theoretical prediction for $v/v_o = 0.04$ according to the model (vide Eq. 13) which is based exclusively on thermal activation and therefore neglects the effects of dislocation drag. In this example only slightly higher values of τ^*/τ_c are required in order to achieve the same velocity when dislocation drag effects are present. For higher values of v/v_c, however, greater increases in τ^*/τ_c are required to compensate for the viscous-drag effects.

The effects of strength of localized obstacles, as represented by $\sin\theta_c$, on the dislocation velocities for a constant temperature are shown in Fig. 10. As the obstacles become weaker and $\sin\theta_c$ becomes smaller, the effects of thermal activation decrease and the average dislocation velocity approaches that given by the drag limit.

Procedures similar to those outlined above can be applied, with only modest increases in analytical complexity, to a synthesis of dislocation-drag mechanisms with that for thermally-activated cutting of localized obstacles when the obstacles are distributed randomly on the slip plane. The synthesis of dislocation-drag mechanisms with those for thermally-activated passage of dislocations over linear obstacles, as e.g. nucleation of kink pairs, presents a more formidable problem that has yet to be solved. A very crude approximation, based on the independent time sequence for each mechanism suggests that.

$$\bar{v} = a\Bigg/\left[\frac{a\,B}{\tau^* b} + \frac{a\,\pi^2\Gamma_o}{\tau_p b^2 L \nu\, \exp\left\{-\frac{2U_k}{kT}\left(1 - \tau^*/\tau_p\right)^n\right\}}\right]^{-1} \qquad [50]$$

where a is the separation of Peierls valleys and the other symbols are defined in Table II. Actual mean dislocation velocities will be slightly less than that given by Eq. 50 due to interactions between the two types of mechanisms.

V. Synthesis of Athermal and Dislocation-Drag Mechanisms. The type of athermal mechanism determines the nature of its effect on dislocation-drag mechanisms. Those athermal mechanisms that depend principally on short-range and long-range order demand that

$$\bar{v} = \frac{\tau^* b}{B} = \frac{(\tau - \tau_{jA})b}{B} \qquad [51]$$

where $j = 1$, or 2, since the athermal back stress is uniformly τ_{jA} along all dislocations. A more complicated relationship results for athermal stresses arising from breaking of attractive junctions. Since, as previously discussed, this effect is though to be small it will not be discussed further here. The effects arising from internal long-range stress fields, however, are significant and can be approximated assuming the usual sinusoidal variation of internal stress over a wave length λ to give an instantaneous dislocation velocity of

$$\frac{dx}{dt} = \frac{(\tau - \tau_{4A}\sin 2\pi x/\lambda)b}{B} \qquad [52]$$

After integrating to obtain the time of transit of the dislocation over one wave length, t_λ, the mean dislocation velocity is calculated to be

$$\bar{v} = \frac{\lambda}{t_\lambda} = \frac{b}{B}\left(\tau^2 - \tau_{4A}^2\right)^{1/2} \qquad [53]$$

The distinction between effects of athermal stresses due to short and long-range order and

long-range internal stress fields on drag-limited velocities are noted in Fig. 11.

VI. Combined Effects of Athermal, Thermally-Activated and Dislocation-Drag Mechanisms. The various pair-wise syntheses of athermal, thermally-activated, and dislocation-drag mechanisms were presented previously to provide a rather direct evaluation of each of the various interaction effects. A unified approach to the evaluation of strain-rate effects where all three major types of mechanisms are simultaneously operative is now easily developed. This will be illustrated for the case where (i) a sinusoidal distribution of internal stress accounts for the athermal stress. (ii) the thermally-activated mechanism consists of activation of dislocation segments over localized barriers distributed in a square array, and (iii) where the drag coefficient B is assumed to have a constant value.

The mean velocity is again given by Eq. 42 and the time t_1, during which the dislocation bows and finally cuts the obstacles by thermal-fluctuations is given by Eq. 47. The sinusoidal variation of the internal stress, however, demands that τ^* of Eq. 45 now be equated to $\tau - \psi\tau_{4A}$ as explained in Sec. III. The free flight time interval, t_2, from the instant of thermal activation to recontact of the dislocation with localized obstacles is now given by

$$t_2 = \frac{L_s - \bar{y}}{\bar{v}} = \frac{B\,(L_s - \bar{y})}{b\,(\tau^2 - \tau_{4A}{}^2)^{1/2}} \qquad [54]$$

where $\bar{y}$ is the average value of y at t_1 and $\bar{v}$ is obtained from Eq. 53. Typical examples of the effects of sinusoidal internal stresses on the velocity-stress relationship for localized barriers of one strength at one temperature are shown in Fig. 12.

VII. Comparison of Experimental Results With Theory. The theoretical predicitions of dislocation velocities and plastic strain rates that were described in the preceeding sections will now be compared with some pertinent experimental data. Three different types of experiments will be discussed, namely (a) determinations of the drag coefficient B from ultrasonic attenuation data, (b) general trends of v as functions of τ and T and estimation of B as deduced form direct measurements of dislocation velocities, (c) and general trends of $\dot{\gamma}$ versus τ for a series of temperatures as obtained from strain-rate tests.

A. Ultrasonic Attenuation Data. Many damping mechanisms contribute to the attenuation of stress waves in crystalline solids. Invariably a portion of the total attenuation in the ultrasonic range arises from dissipation of mechanical energy due to the operation of dislocation-drag mechanisms. Analyses of such attenuation data are usually based on the vibrating string model introduced by Koehler (99), elaborated by Granato and Lucke (100,111), and further refined by Rogers (102). A significant assumption made in this model is that the drag force normal to each unit length of a moving dislocation is linearly related to its velocity as given by Bv. In general the attenuation depends on the amplitude of vibration and distribution of dislocation segment lengths. Most tests for the determination of B, however, have been conducted in the low-amplitude and high-frequency range of conditions where the experimental results and deductions based on the Granato Lucke model agree in giving attenuations that are independent of amplitude and loop length. Under these conditions

$$B = 2\,\Omega\,\rho\Gamma_o/\delta_c \qquad [55]$$

where Ω is an orientation factor, ρ is the density of the freely vibrating dislocations and δ is the limiting attenuation at very high frequencies arising from dislocation-drag mechanisms. Mason (103) has summarized the various methods that have been employed to separate the dislocation-drag effects that account for δ from the total attenuation from all causes. Although ρ refers only to the density of the freely vibrating dislocations, it is usually estimated in terms of etch-pitting or x-ray techniques which approximate the total dislocation density.

Recently Hikata and Elbaum (86) have determined the attenuation in normal and superconducting Pb at low temperatures in the high-amplitude and high-frequency region where the attenuation is amplitude dependent and increases linearly with frequency. Their evaluation of B was based on Roger's extension of the string model to include large amplitudes so as to account more accurately for breakaway of pinned dislocation segments. The maximum attenuation occurs for stress amplitudes where dislocation breakaway from pinned points first becomes complete, additional increases in the stress amplitude cause no further losses due to breakaway, and therefore result in decreases in attenuation for yet greater amplitudes.

The maximum attenuation for the superconducting state occurred at lower amplitudes than that for the normal state, thus accounting for lower values of B for the superconducting state. This effect is attributable to lowered damping in the superconducting state arising from uncoupling of electrons from the phonons. The shift in amplitude at maximum attenuation was used to determine B. The analysis did not need to invoke any ad hoc assumptions concerning details of dislocation networks. The values of B so obtained for the normal state were essentially independent of temperature over the range from 4.2°K to about 15°K. Although these data are inconsistent with expectations based on Mason's (78-80) estimate for electron viscosity, they are in accord with Holsteins (75) model for electron scattering.

Available data from attenuation investigations are summarized in Table V. and show that B usually ranges from 0.5 to about 20 x 10^{-4} dynes-sec/cm^2.

B. Direct Measurements of Dislocation Velocities. The Johnston-Gilman Technique (113) and modifications thereof are used for direct determination of dislocation velocities. This involves dividing the displacement of specially introduced mobile dislocations by the duration of an applied stress pulse. Dislocation displacements are determined either by etch-pitting or by the Berg-Barrett x-ray technique. The latter has the advantage of not only being more generally applicable but also giving additional information regarding Burgers vectors of the dislocations involved. Experiments by Johnston and Gilman (113) and Gorman, Wood and Vreeland (114), have demonstrated that the same velocities are obtained from pulses of the same intensity regardless of their duration, revealing that the inertia of dislocations is extremely small and thus confirming the nominal validity of this simple method for determining dislocation velocities.

Inaccuracies in the velocity-stress data arise from a series of causes: (a) Stress pulses, particularly those of short duration at the higher stresses, often deviate appreciably from the idealized rectangular shape. Corrections usually made to compensate for such pulses are crude except for cases that approach the idealized condition such as result when torsional shock bar techniques (115) are used. (b) Velocities show wide scatter from specimen to specimen depending on variations in perfection of crystal substructure. For example acid machined specimens usually give higher velocities (116) than those prepared by spark erosion techniques. (c) Variations in velocities of different dislocations are also obtained in a single test. Such scatter is often attributable to the presence of nearby dislocations, local differences in their arrangements and consequent effects arising from local differences in the internal stress fields. Usually no corrections were applied so as to compensate for such variations. In a few cases corrections were attempted but the methods employed were crude and of questionable validity and accuracy. (d) Velocities were reported as mean values in some investigations and as the maximum values obtained in others. Both measures reflect in different ways variations that arise from techniques of introducting mobile dislocations and local differences on surface conditions. It is difficult to satisfactorily justify either measure of velocity.

Dislocation velocities are usually reported as functions of the applied stress. Over the low-stress range, as emphasized by investigations referred to in Table VI A, dislocation velocities follow the general trends with variations in temperature and stress that are expected when thermally-activated mechanisms control dislocation motion. Confirmation and detailed analyses of the operative mechanism requires information on the variations in

TABLE V

Damping Coefficient B

Crystal	B x 10^4 dyne-sec/cm^2	Temp °K	Dislocation density, cm^{-2}	Ref.
LiF	2.4	300	3 x 10^7	(104)
	3.4	300	8 x 10^5	(105)
	7.0	300	5 x 10^6	(112)
NaCl	4.5	300	-	(106)
	1.6	300	1.2 x 10^7	(104)
Al	14.5	77	5 x 10^6	(107)
	12.0	100		
	11.0	150		
	12.5	195		
	16.0	300		
Cu	2.24	100	4.3 x 10^6	(108)
	4.0	180		
	7.5	300		
Cu	0.58	77	4 x 10^6	(112)
	1.2	298		
	2.2	400		
Cu	6.5	300	2.5 x 10^6	(109)
Pb	3.7	300	2.4 x 10^7	(110)
	1.24	77	"	
Pb	0.86	4.2°K	-	(111)

activation energies and activation areas with the effective stresses. In most investigations, however, no attempt was made to determine activation energies or the athermal stress level that is needed to calculate the effective stresses. These omissions coupled with inaccuracies and scatter in dislocation velocity data have compounded the difficulties encountered in attempting detailed identification of the thermally-activated mechanism. The data reported by Prekel and Conrad (123) on the velocities of dislocations in Mo constitute a noteworthy exception to the usual investigations. They determined the athermal stress level and reported velocities in terms of the effective stress. As will be discussed in greater detail in the following section, Prekel and Conrad showed that velocity data obey the same relationships as strain-rate data.

TABLE VI A

Dislocation Velocity (Low Stress Region only)

Crystal	Ref.	Temperature °K	Stress Range dy/cm^2	Velocity Range cm/sec	Remarks
Ge	(117)	713, 773, 823, 873, 973	1×10^8 to 5.5×10^8	5×10^{-6} to 10^{-1} M;EP	No orientation dependence of velocity
3.25% Si-Fe (110) slip	(118)	78, 198, 298, 373	1 to 3×10^9	3×10^{-8} to 10^{-2}; M;EP	8 microns substracted from traverse.
3.25% Si-Fe (112) slip	(119)	198, 233, 298	1.25 to 2.2 $\times 10^9$	10^{-7} to 10^{-2}; M;EP	26 micron substracted from traverse
Nb	(120)	300, 194, 77	1.6×10^8 to 5.1×10^9	2×10^{-7} to 3×10^{-1} A;EP	Neutron irradiation had the same effect as lowering temp.
Fe	(121)	77, 198, 295, 373	1.2×10^7 to 5.4×10^8	3.7×10^{-7} to 10^{-1} A;Xr	Measurements made on slip bands, not on individual disl.
Zn pyramidal slip	(122)	77, 88, 100 110, 175, 230, 273, 294, 323	3.6 to 65.5 $\times 10^6$	10^{-6} to 10^{-1} M;EP + XR	In the low temperature region, screw dislocation moves faster than edge.
Ni	(123)	77, 153, 273	0.3 to 1.0 $\times 10^8$	4×10^{-7} to 10^{-2}; A;EP	Motion of edge dislocation observed; 8 micron substracted from traverse.
Mo	(124)	300	0.6 to 2.5 $\times 10^8$	7×10^{-7} to 5×10^{-3} M;EP	Dislocation moved only on {112} planes.

A = Average velocity; M = maximum velocity; EP and XR are etch pit and x-ray method for observing position of dislocation respectively.

Dislocation velocity data that extend into the high stress range are summarized in Table VI B. Velocities in excess of about 10^3 cm/sec appear to be almost linearly

TABLE VI B

Dislocation Velocity (With Emphasis on High Stresses)

Crystal	Ref	Stress range dy/cm^2	Velocity range cm/sec	Temp °K	†B x 10^4 dyne-sec/cm^2	Remarks
NaCl	(125)	2.0×10^6 to 5.0×10^8	2×10^{-8} to 2×10^4 A;EP	300	2.0	Edge dislocations moved faster than screws.
LiF	(126)	6×10^7 to 1.96×10^9	4×10^{-6} to 6.5×10^4; A;EP	300 77	7.0	Edge dislocations moved faster than screws at lower stresses
Al	(127)	up to 1.6×10^7	10^1 to 2.8×10^3; M;XR	74 123 173 296	1.33 1.5 1.9 2.4	Velocity measured in (111) plane; Large Scatter in data.
Cu	(128)	2×10^6 to 1.4×10^7	1.5×10^2 to 6.2×10^2; M;XR	296	7.0	Edge dislocation velocity measured
Cu	(129)	7×10^5 to 4.5×10^6	up to 8×10^2	77 298	1.4	Non-uniform motion of dislocations
Zn (basal slip)	(130)	up to 1.7×10^7	4.0×10^2 to 7.0×10^2; M;XR	300	7.0	Predominantly edge disl; stress pulse not rectangular
Pb	(131)	10^7 to 5×10^8	up to 5.5×10^4;M	78 300	2.22 3.43	Measurments made on slip band

† B is measured from the linear plot of velocity - stress data in the high stress region.

dependent on the applied stress suggesting that the dislocation drag mechanisms is operative in this region. Early suggestions (113) that the highest of these velocities were approaching the relativistic limit of that for sound have proved to be incorrect. As shown in Fig. 8 theoretical curves of velocity versus stress exhibit two regions where the velocity increased somewhat linearly with stress. The first occurs in the steep part of the v - τ curve characteristic of where the rate controlling mechanisms is changing from principally thermally-activated to the dislocation-drag mechanisms. The second occurs at the highest stresses where dislocation velocities are principally controlled by dislocation-

drag mechanisms. Even at relatively high velocities the slopes of the $v - \tau$ curves depend somewhat on the activation energies, temperature and the athermal stress level. In the past the effects of these variables on the $v - \tau$ relationship were neglected and the drag coefficient was evaluated as $B = (\tau_2 - \tau_1)\, b/(v_2 - v_1)$ where v_2 and v_1 are velocities associated with τ_2 and τ_1 respectively in the high velocity linear range. Usually, however, athermal stress levels are small relative to the applied stresses in this range. Typical experimental results of v versus τ curves in the high stress range are shown in Fig. 13. Typical values of B obtained from velocity investigations are listed in Table VI B. Admitting various inaccuracies these values agree reasonably well with those deduced from acoustic attenuation measurements previously presented in Table V.

C. Strain-Rate Effects. Various types of experimental techniques have been used to determine the effects of stress, temperature, strain-hardening, structure and substructure etc., on plastic strain rates. Such techniques fall naturally into one of two major groups dependent on the magnitude of the strain rate. For slow strain rates, up to about 10 per second, either constant stress type creep tests or, more often, constant strain-rate tests (tension, compression and shear) are well adapted to give accurate and correlatable data. For the higher strain rates, which might range from about 10^2 to almost 10^5, various types of dynamic impact test methods have been employed, among them the Kolsky technique (132) and modifications thereof. As the strain rate is increased, the techniques of measurement become more complicated. Often considerations of the presence of inertial stresses and wave propagation effects are overlooked thus leading to less accurate data than those reported for the lower strain rates. New or better experimental techniques need yet be developed to provide satisfactory accuracy for cases where the strain rates exceed about 10^5 per second.

As shown by Eq. 11, plastic strain rates are linearly related to the product of the Burgers vector, the mobile dislocation density and the mean velocity of such mobile dislocations. Whereas v can be evaluated as a function of the effective stress and temperature by direct measurement, no experimental technique has yet been developed to determine ρ during a test. During strain-hardening in the athermal region it is known that the total dislocation density increases as the square of the athermal stress level, given by Eq. 20. Within the limits of experimental scatter the same conditions hold during high-temperature steady-state diffusion - controlled creep. In addition the steady-state rates obtained during Viscous Glide creep agree extremely well with the theoretical predictions based on the hypothesis that the mobile dislocation density is equal to the total dislocation density which obeys Eq. 20. On the other hand, as demonstrated by Johnston and Gilman (113) and also Hahn (133), when the initial mobile dislocation density is much below that suggested by Eq. 20 (where now τ refers to the yield stress) dislocation multiplication takes place upon deformation, the stress-strain curve exhibits a yield point and finally following yield straining, the correlations given by Eq. 20 become valid. In general, however, ρ cannot change unless either straining or recovery takes place. In analyses of most strain-rate data the assumption is usually made that ρ is constant for a given strain hardened state, despite the increase in flow stress with decreasing test temperature. This assumption is wholly consistent with the previously quoted correlations. Furthermore Prekel and Conrad (124) have shown that the experimental values of $\partial(\ln\dot{\gamma})/\partial\tau$ and $kT(\partial\ln v/\partial\tau)$, at constant temperature, deduced independently from strain-rate and dislocation velocity tests respectively on Mo are within experimental error identical functions of the effective stress τ^*. If the mobile dislocation density had increased with τ^2, the calculated value of $kT(\partial\ln\dot{\gamma}/\partial\tau)$ should have exceeded that for $\partial\ln v/\partial\tau$ by $2\,kT/\tau$. At $T = 300°$ and $\tau = 1$ kg/mm^2, $kT(\partial\ln\dot{\gamma}/\partial\tau)$ should have exceeded $kT(\partial\ln v/\partial\tau)$ by 30%. Since this discrepancy is greater than the experimental error it follows that the mobile dislocation density, for these tests conducted at a fixed state, does not vary as τ^2 but remains substantially constant. In many high strain-rate dynamic tests however, it is customary for the sake of accuracy to first correlate the strain rate with stress following about one percent or more of straining. Therefore if Eq. 20 were also expected to apply in these tests, the strain rate should have increased with about the third power of the stress. In contrast, however, at strain rates where dislocation drag mechanisms seem to be rate controlling, the strain rate

increases almost linearly with the effective stress. The reasons for this apparent discrepancy have not yet been resolved. But when either the theoretically estimated or the experimentally determined value for v is introduced into Eq. 11, ρ is estimated to have the not too unreasonable value of about 10^7 per cm^2 over a rather wide range of stresses.

Experimental data on strain-rate versus stress relations over a wide range of strain rates are now available on Al (131-139) and Al-Cu alloy (138), Cu (140,141) AgMg (142), Ag_2Al (143), Zn (144-145) and mild steels (146). An example is given in Fig. 14 illustrating recent results for Al (137). The general trends coincide with those suggested by the sythesis of athermal, thermally activated, and dislocation-drag mechanisms as shown in Fig. 12. Despite the nominal agreement, the observed strain-rate versus stress relationship usually fails to exhibit the inversion noted in the theoretical curves of Fig. 8, 10 and 12 over the transition region from the thermally-activated to the dislocation drag region; in addition, the slope of the experimental curves increases with increasing temperatures whereas the theoretical curves exhibit the opposite trend. These second order differences between experiment and theory need yet be resolved.

VII SUMMARY

The laws for plastic flow in crystalline solids are usually quite complicated and frequently appear to vary from one solid to another. These facts are now known to be reflections of the hosts of different deformation mechanisms crystalline solids undertake.

Four major types of deformation mechanisms, (a) diffusion-controlled creep, (b) athermal, (c) thermally-activated, (d) and dislocation-drag processes, are now clearly identified and documented. All four major types of mechanisms however, contribute simultaneously to the observed net strain-rate effects. The complexity of the plastic behavior of crystalline solids is further enhanced by the fact that a number of different individual subtype mechanisms usually operate at the same time so as to contribute to the observed effect of each major type of mechanism. Only in certain simple examples, and then only over special limited ranges of experimental conditions, may the influence of only one of the operative mechanisms predominate. Despite the excellent progress that has been made, especially recently, in rationalizing strain-rate effects, much yet remains to be completed: (a) An area of considerable interest concerns the replacement of simple string models for dislocations by more realistic models based on atomic interactions. Such advances would provide improved concepts of dislocation interactions with each other and other strain centers, and better predictions on stacking fault energies, energies for cutting localized obstacles, and forming constrictions, jogs, etc. These advances should also provide a clearer picture of the motion of dislocations over Peierls hills and for the failure of the Schmidt Laws in bcc metals. (b) In addition a great need exists for the development of geometric probability appropriate to dislocation dynamics so as to permit rationalization of thermally activated behavior of dislocations past a random distribution of localized obstacles and when several mechanisms are simultaneously operative (c) The attempt to obtain a unified analytical structure for visualizing the combined effects of the four major dislocation mechanisms, given major emphasis in this report, need be pursued to much greater depth. (d) Each of the four major types of deformation mechanisms require additional theoretical development and experimental exploration. (e) Because no analyzable experimental data are available for strain-rate effects where the dislocation velocities are in the relativistic or the supersonic ranges, this should prove to be a fruitful area for research. Additional theoretical developments are also needed in this range.

Acknowledgement

The authors express their appreciation to the United States Atomic Energy Commission for their support of this investigation through the Inorganic Materials Research Division of the Lawrence Radiation Laboratory of the University of California.

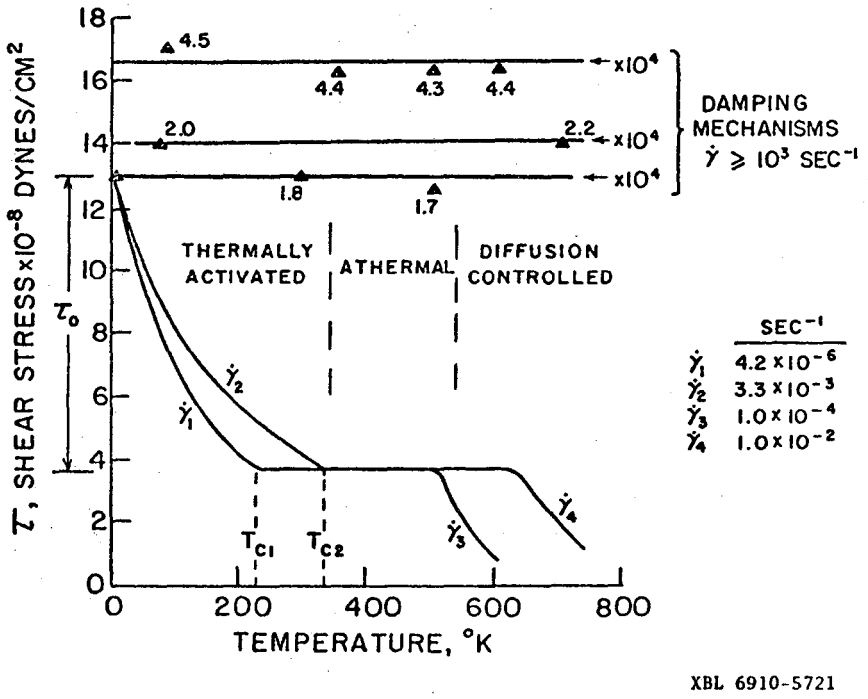

FIG.1
Temperature and Strain-Rate Range for the Four Major Types of Dislocation Mechanisms. (AgMg Monocrystals)

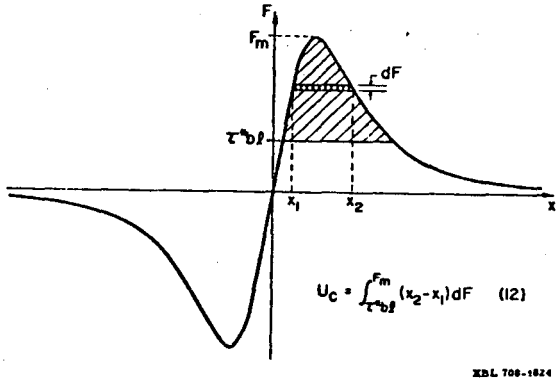

FIG. 2
Force - Displacement Diagram and Free Energy of Activation, U_c, for Cutting Localized Obstacles.

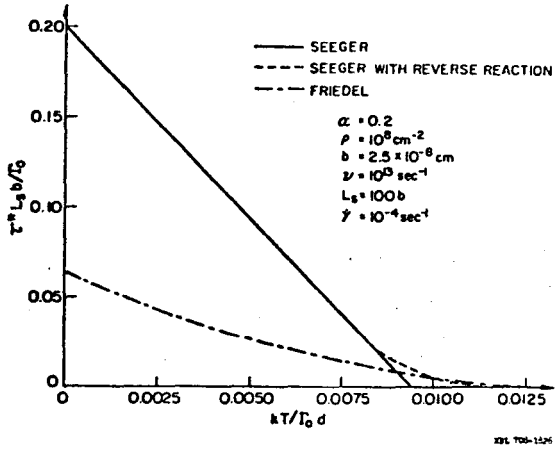

FIG. 3
Effects of Reverse Activation and Friedal Steady-State Approximation for Random Distribution of Localized Obstacles on the τ*-T Relationship.

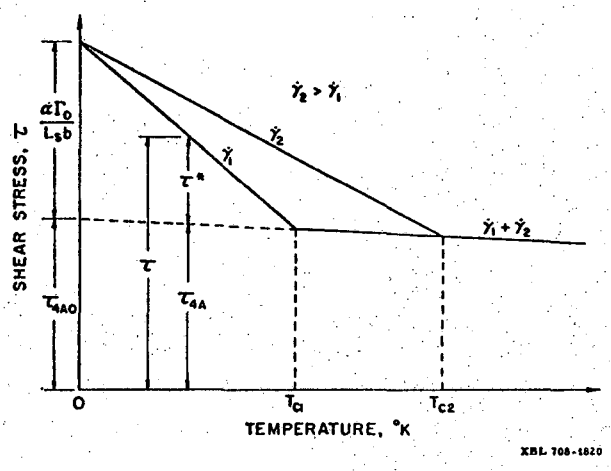

FIG. 4A
Intersection Mechanism Assuming Superposition so that $\tau = \tau^* + \tau_{4A}$.

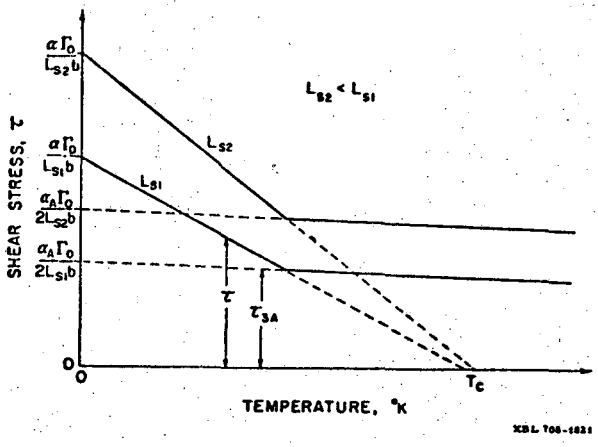

FIG. 4B
Intersection Mechanism Assuming Athermal Stress Arises from Cutting Attractive Junctions.

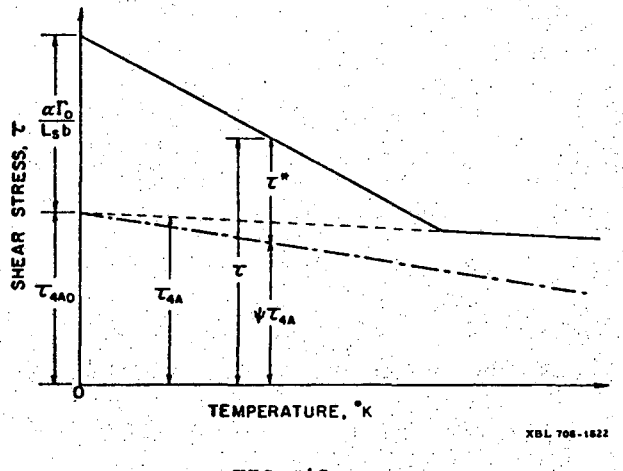

FIG. 4C
Intersection Mechanism Assuming Athermal Stress Level due to Internal Stresses $\tau_i = \tau_{4A} \sin 2\pi x/\lambda$.

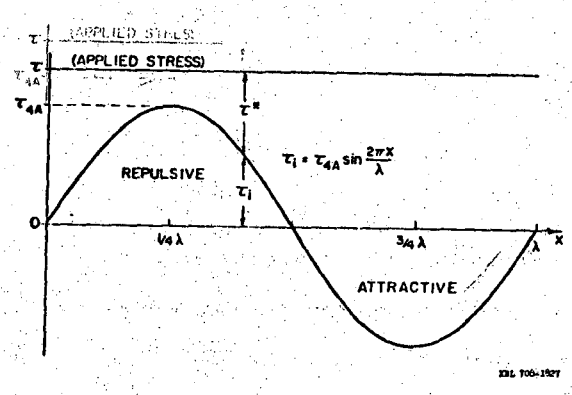

FIG. 5
Effective Stress τ^* Due to Internal Stress Field $\tau_i = \tau_{4A} \sin 2\pi x/\lambda$.

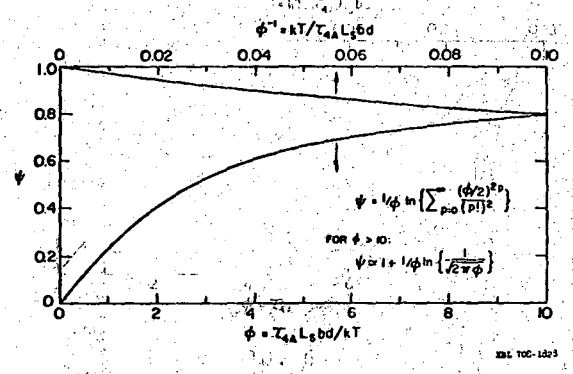

FIG. 6
Average Effective Stress, $\bar{\tau}^* = \psi\tau_{4A}$ — Sinusoidal Internal Stresses.

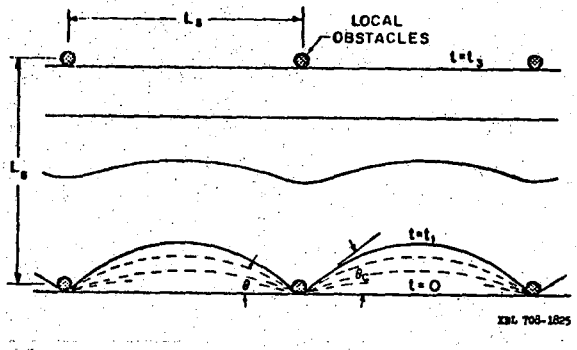

FIG. 7
Thermal Activation Past Square Array of Localized Obstacles Followed by Dislocation-Drag to Next Set of Obstacles.

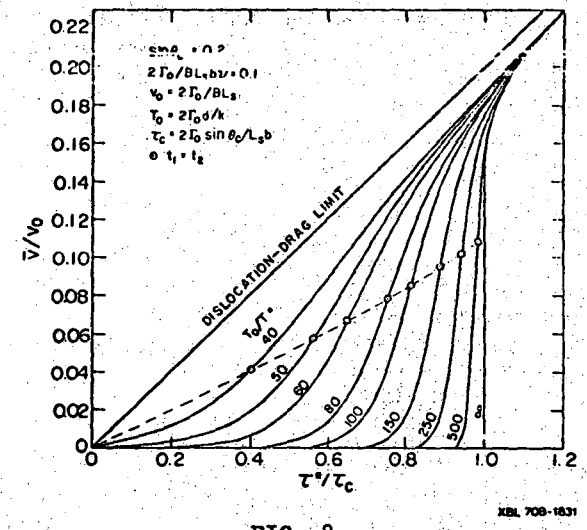

FIG. 8
Dislocation Velocity versus Effective Stress at Series of Temperatures for Thermal-Activation and Dislocation-Drag Mechanisms.

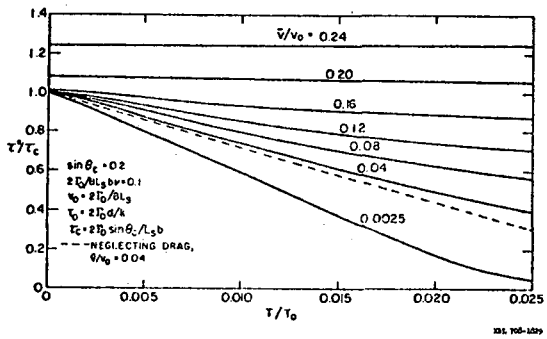

FIG. 9
τ^*–T Relationship at Constant Velocities Assuming Thermally-Activated and Dislocation-Drag Mechanisms.

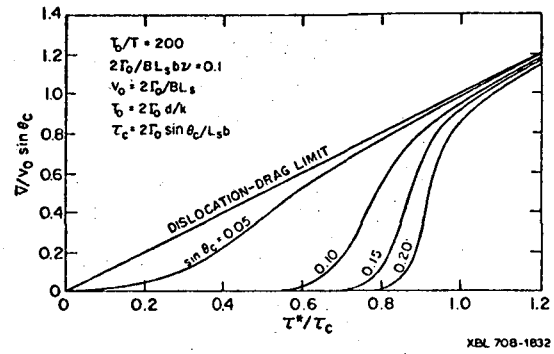

FIG. 10
Velocity-Effective Stress Relationship for a Series of Obstacle Strengths at one Temperature.

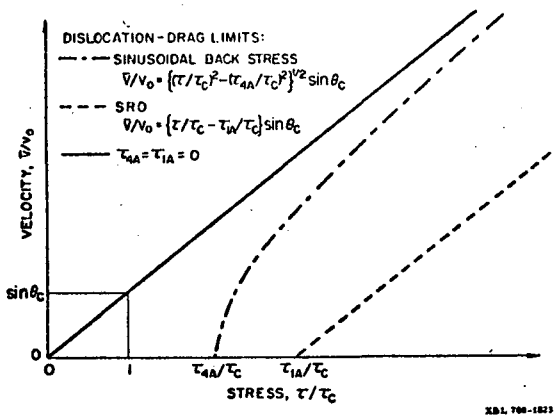

FIG. 11
Effect of Back Stresses and Sinusoidal Internal Stresses on the Dislocation-Drag Limit.

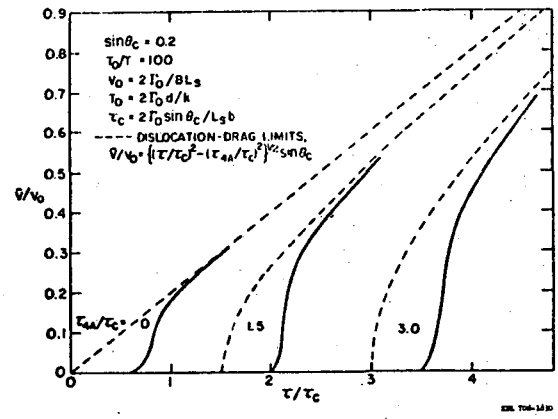

FIG. 12
Combined Effects of Sinusoidal Internal-Stress Fields, Thermal Activation over Obstacles and Dislocation-Drag Mechanisms.

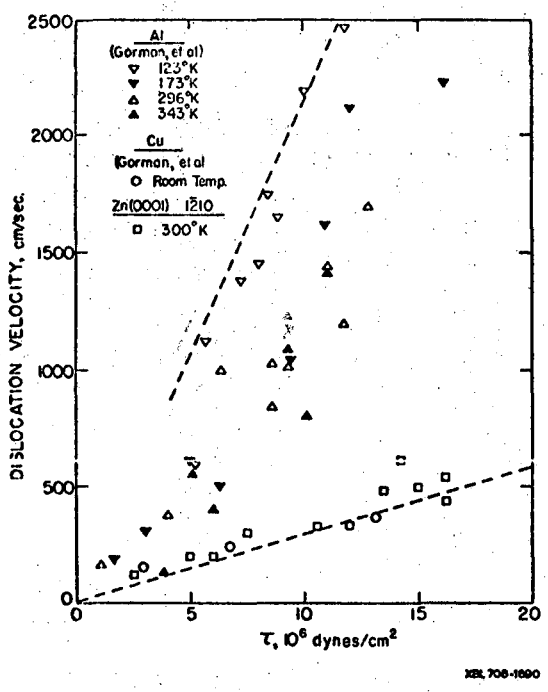

FIG. 13
Dislocation Velocity Versus Stress.

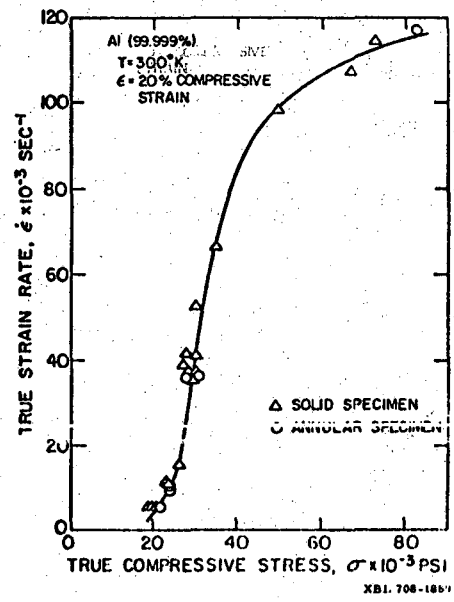

FIG. 14
Strain Rate Versus Stress.

References

1. John E. Dorn, "Low-Temperature Dislocation Mechanisms," in Dislocation Dynamics, Ed. A. R. Rosenfield et al., McGraw-Hill Book Co., New York, p. 27-55 (1968).

2. A. K. Mukherjee and J. E. Dorn, J. Inst. of Metals, 93, 397 (1964-65).

3. A. K. Mukherjee and J. E. Dorn, Trans. Met. Soc. AIME, 230, 1065 (1964).

4. A. K. Mukherjee, W. G. Ferguson, W. L. Barmore and J. E. Dorn, J. Appl. Phys., 37, 3707 (1966).

5. J. E. Bird, A. K. Mukherjee, and J. E. Dorn, "Correlations Between High-Temperatures Creep Behavior and Structure," in Quantitative Relation Between Properties and Microstructure, Israel University Press, Jerusalem, p. 255-342, (1969).

6. F. R. N. Nabarro, Report of a Conference on the Strength of Solids, p. 75, The Physical Society, London (1948).

7. R. L. Coble, J. Appl. Phys. 34, 1679 (1963).

8. J. Weertman, J. Appl. Phys. 28, 362 (1947).

9. J. Weertman, Trans. ASM, 61, 681 (1968).

10. J. Weertman, J. Appl. Phys., 28, 1185 (1957).

11. A. H. Cottrell, "Dislocations and Plastic Flow in Crystals," p. 136, Claredon Press, Oxford (1953).

12. H. Suzuki, Sci. Rep. Res. Inst., Tohoku Univ. (Japan), 7A, 194 (1955).

13. J. Fisher, Acta Met. 2, 9 (1954).

14. S. L. Robinson and O. D. Sherby, Acta Met., 17, 109 (1969).

15. K. E. Amin, A. K. Mukherjee and J. E. Dorn, "A Universal Law for High-Temperature Diffusion controlled Transient Creep", to be published in J. of Mech. and Phy. of Solids.

16. J.C.M.Li., Canad. J. Phy., 45, 493 (1967); Dislocation Dynamics, p. 87 Ed. A., Rosenfield et al, Mc-Graw Hill, N. Y., (1968).

17. G. Schoeck, Phy. Stat. Sol., 8, 499 (1965).

18. J. P. Hirth and W. D. Nix, "An Analysis of the Thermodynamics of Dislocation Glide", Rep. No. SU-DMS-69-R-45, Dept. of Matl. Sc., Stanford University, (1969).

19. G. B. Gibbs, Phy. Stat. Sol. iv, 507 (1965); Phil. Mag. 16, 97 (1967); Mat. Sc. Engr. 4, 312, (1969).

20. R. Peierls, Proc. Phys. Soc. 51, 34 (1940).

21. A Seeger, Phil. Mag. 1, 651 (1956).

22. J. Friedel, "Electron Microscopy and Strength of Crystals," p. 605, Interscience Publishers, 1963.

23. V. Celli, M. Kabler, T. Nimoiya and R. Thomson, Phys. Rev. 131, 58 (1963).

24. J. Dorn and S. Rajnak, Trans. Met. Soc. AIME, 230, 1052 (1964).

25. P. Guyot and J. E. Dorn, Canad. J. of Phys. 45, 983 (1967).

26. J. E. Dorn and A. K. Mukherjee, Trans. Met. Soc. AIME, 245, 1493 (1969).

27. A. Seeger, Phil. Mag. 45, 771 (1954).

28. J. Friedel, "Dislocations," p. 264, Pergamon Press, Oxford, (1964).

29. B. Escaig, Proc. Phys. des Disl., Toulouse (1966).

30. A. Cottrell, Phil. Mag., 43, 645 (1952).

31. N. Mott, Phil. Mag., 43, 1151 (1952).

32. A. Cottrell, J. Mech. and Phys. Sol. 1, 53 (1952).

33. A. Seeger, Phil. Mag., 46, 1194 (1955).

34. Z. S. Basinski, Phil. Mag., 4, 393 (1959).

35. J. Friedel, "Dislocations," p. 121 and 221, Pergamon Press, Oxford, 1964.

36. A. Cottrell and B. Bilby, Proc. Phys. Soc., A62 49 (1949).

37. N. Mott and F. R. N. Nabarro, Proc. Phys. Soc., 52, 84 (1940).

38. A. Cochardt, G. Schoeck and H. Wiedersich, Acta Met. 3, 533 (1955).

39. R. Fleischer, Acta Met. 10, 835 (1962).

40. R. Fleischer and W. Hibbard, "The Relation Between the Structure and Mechanical Properties of Metals," p.262, Her Majesty's Stationery Office, London (1963).

41. J. Friedel, "Dislocations," p. 351, Pergamon Press, Oxford (1964).

42. A. Kelly and M. Fine, Acta Met. 5, 365 (1957).

43. R. Fleischer, Acta Met. 8, 32 (1961).

44. M. Fine, "The Relation Between the Structure and Mechanical Properties of Metals," p. 299, Her Majesty's Stationery Office, London (1963).

45. J. Friedel, "Dislocations," p. 376, Pergamon Press, Oxford (1964).

46. A. Seeger, Proc. 2nd U.N. International Conf. PUAE, 6, 250 (1958).

47. A. Seeger, Radiation Damage in Solids, IAGA, 1, 101 (1962).

48. J. Diehl and W. Shilling, Proc. 3rd U.N. International Conf. PUAE, 9, 72 (1964).

49. J. Diehl, G. Seidel, and L. Nieman, Phys. Stat. Sol. 11, 339 (1965), Phys. Stat. Sol. 12, 405 (1965).

50. W. Frank, Phy. Stat. Sol. 26, 197 (1968).

51. Z. S. Basinski, Phil. Mag., 4, 393 (1959).

52. J. Friedel, "Dislocations," p. 224, Pergamon Press, Oxford (1964).

53. J. E. Dorn and A. K. Mukherjee, "Application of Rate Theory to Dislocation Dynamics," presented at the AIME Symposium on Thermal and Non-Thermal Crystalline Deformation, Philadelphia, Oct. 1969; Rep. no. UCRL-19097, Lawrence Radiation Laboratory, University of California, Berkeley.

54. A. H. Cottrell, "Relation of Properties to Microstructure," p. 131, Amer. Soc. Metals, Cleveland, Ohio (1954).

55. G. Saada, Acta Met. 8, 841 (1960).

56. G. Saada, Acta Met. 9, p. 2 and 160 (1961).

57. G. Saada, Electron Microscopy and Strength of Crystals, p. 651, Interscience Publishers, New York (1963).

58. P. Guyot, Acta Met., 14, 955 (1966).

59. G. Taylor, Proc. Roy. Soc. London, 145A, 362 (1934).

60. N. Mott, Phil. Mag., 43, 1151 (1952).

61. A. Seeger, J. Diehl, S. Mader and H. Rebstock, Phil. Mag. 2, 323 (1957).

62. A. S. Keh and S. Weissman in "Electron Microscopy and Strength of Crystals", p. 231, J. Wiley. N. Y. (1963).

63. A. Foreman and M. Makin, Phil. Mag. 14, 911 (1966).

64. J. Weertman, "High Velocity Dislocations," in Response of Metals to High Velocity Deformation, p. 205, Interscience, New York (1960).

65. A. N. Stroh, J. Math. Phys. 41, 77 (1962).

66. J. Weertman, J. Appl. Phys. 33, 1631 (1962).

67. J. Weertman, J. Mech. Phys. Solids 11, 197 (1963).

68. J. Weertman, J. Appl. Phys. 38, 5293 (1967).

69. J. Eshelby, Proc. Roy. Soc. London, A197, 789 (1956).

70. A. Granato and K. Lucke, J. Appl. Phys. 27, 789 (1956).

71. J. Eshelby, Proc. Roy. Soc. London, A197, 396 (1957).

72. G. Liebfried, Z. Physik 127, 344 (1950).

73. J. Eshelby, Proc. Roy. Soc. London, A266, 222 (1962).

74. J. Lothe, J. Appl. Phys. 33, 2116 (1962).

75. T. Holstein, Appendix to paper by B. R. Titman and H. E. Bommel, Phys. Rev. 151, 178 (1966).

76. V. Ya. Kravchenko, Soviet Physics-Solid State, 8, 740 (1966).

77. A. Akheiser, J. Phys. USSR, 1, 277 (1939).

78. W. Mason, J. Acous. Soc. Amer. 32, 458 (1960).

79. W. Mason and T. Bateman, J. Acous. Soc. Amer. 36, 644 (1964).

80. W. Mason, J. Appl. Phys. 35, 2779 (1964).

81. W. Mason, Phys. Rev. 97, 557 (1955).

82. W. Mason, Phys. Rev. 143, 339 (1966).

83. B. R. Titman and H. E. Bommel, Phys. Rev. 151, 178 (1966).

84. W. P. Mason and A. Rosenberg, J. Appl. Phys. 38, 1929 (1967).

85. W. P. Mason, "Dislocation Dynamics," p. 487, Ed. A. R. Rosenfield, McGraw-Hill Co., New York, 1968.

86. A. Hikata and C. Elbaum, Supplement to Transactions to the Japan Inst. of Metals 9, 46 (1968).

87. A. Hikata, R. A. Johnson and C. Elbaum, Phys. Rev. Letters 24, 215 (1970).

88. A. Cottrell and R. Stokes, Proc. Roy. Soc. London, A233, 17 (1955).

89. W. D. Nix, W. A. Coghlan and C. R. Barrett, Mat. Sci. Eng. 4, 98 (1969).

90. H. S. Chen, J. J. Gilman and A. K. Head, J. Appl. Phys. 35, 2502 (1964).

91. K. R. Evans, D. J. Bailey and W. F. Flanagan, Phys. Stat. Sol. 22, 607 (1967).

92. R. J. Arsenault and J. C. M. Li, Phil. Mag. 16, 1307 (1967).

93. K. H. Adams, J. Appl. Phys. 30, 4040 (1968).

94. J. C. M. Li, Dislocation Dynamics, Ed. A.R. Rosenfield, McGraw-Hill, N. Y. p. 87 (1968).

95. A. Argon, Mat. Sci. Eng. 3, 24 (1968).

96. F. C. Frank, Proc. Phys. Soc. London, A62, 131 (1949).

97. H. J. Frost and M. F. Ashby, "The Motion of a Dislocation Acted on by a Viscous Drag through an Array of Discreet Obstacles," Tech. Reps. No. 1, March, 1970. Div. of Eng. and Appl. Phys., Harvard Univ., Cambridge, Mass.

98. H. S. Carslaw and J. C. Jaeger, "Conduction of Heat in Solids," p. 130, Claredon Press, Oxford (1959).

99. J. S. Koehler, "Imperfections in Nearly Perfect Crystals, p. 197, Eds. W. Shockley et al., John Wiley, New York (1952).

100. A. Granato and K. Lücke, J. Appl. Phys. 27, 583 (1956).

101. A. Granato and K. Lucke, J. Appl. Phys. 27, 789 (1956).

102. D. H. Rogers, J. Appl. Phys. 33, 781 (1962).

103. W. P. Mason, "Microplasticity," p. 287, Ed. C. J. McMahon, Jr., Interscience, New York, (1968)

104. F. Fanti, J. Holder and A. V. Granato, J. Acoust. Soc. Amer. 45, 1356, (1969).

105. O. M. M. Mitchell, J. Appl. Phy., 36, 2083, (1965).

106. R. A. Moog, "Utransonic Adsorption in NaCl". Ph.D. Thesis, Cornel Univ. (1965).

107. W. P. Mason and A. Rosenberg, Phy. Rev., 151, 434, (1966).

108. G. A. Alers and D. O. Thompson, J. Appl. Phy., 32, 283, (1961).

109. R. M. Stern and A. V. Granato, Acta Met. 10, 358, (1962).

110. W. P. Mason and A. Rosenberg, Appl. Phy., 38, 1929, (1967).

111. A. Hikata and C. Elbaum, Trans. J. Inst. Met., Japan, 9, 46, (1968).

112. T. Suzuki, A. Ikushima and M. Aoki, Acta. Met., 12, 1231, (1964).

113. W. G. Johnston and J. J. Gilman, J. Appl. Phys. 30, 129 (1959).

114. J. A. Gorman, D. S. Wood and T. Vreeland Jr., J. Appl. Phys. 40, 833 (1969).

115. D. P. Pope, T. Vreeland Jr., and D. S. Wood, Rev. Sci. Inst. 35, 1351 (1964).

116. K. H. Adams, R. C. Blish and T. Vreeland Jr., Mat. Sci. Eng. 2, 201 (1967).

117. A. R. Chandhuri, J. R. Patel and L. G. Rubin, JAppl. Phy., 33, 2736 (1962).

118. D. F. Stein and J. R. Low, J. Appl. Phy., 31, 362 (1960).

119. J. S. Erickson, J. Appl. Phy., 33, 2499, (1962).

120. H. D. Guberman, Acta. Met., 16, 713 (1968).

121. A. P. L. Turner and T. Vreeland Jr., W. M. Keck Laboratories, Calif. Inst. of Technology, Pasadena, Calif. Report no. Calt 767-P3-7.

122. R. C. Blish II and T. Vreeland Jr., J. Appl. Phy. 40, 884, (1969).

123. R. W. Rhode and C. H. Pitt, J. Appl. Phy. 38, 876, (1967).

124. H. L. Prekel and H. Conrad, "Dislocation Dynamics", Ed. A. R. Rosenfield et al., McGraw-Hill, P. 431, (1968).

125. E. Yu. Gutmanas, E. M. Nadgornyi and A. V. Stepanov, Soviet Physics - Solid State, 5, 743, (1963).

126. W. G. Johnston and J. J. Gilman, J. Appl. Phy. 30, 129, (1959).

127. A. Gorman, D. S. Wood and T. Vreeland Jr., J. Appl. Phy. 40, 833, (1969).

128. T. Vreeland Jr., "Dislocation Dynamics", Ed. A. R. Rosenfield et al., McGraw-Hill, p. 529, (1968).

129. Suzuki, "Dislocation Dynamics", ed. A. R. Rosenfield, McGraw-Hill, N.Y., p. 551, (1968).

130. D. P. Pope, T. Vreeland Jr. and D. S. Wood, J. Appl. Phy, 38, 4011, (1967).

131. V. R. Parameswaran and J. Weertman, Scripta Met. 3, 477, (1969).

132. H. Kolsky, Proc. Phys. Soc. Sec. B, 62, 676 (1949).

133. G. T. Hahn, Acta Met. 10, 727 (1962).

134. F. E. Hauser, J. A. Simmons, J. E. Dorn, "Response of Metals to High Velocity Deformation," p. 93, Ed. V. F. Zackay, Interscience (1961).

135. W. G. Ferguson, A. Kumar and J. E. Dorn, J. Appl. Phys. 38, 1863 (1967).

136. A. Kumar, F. E. Hauser and J. E. Dorn, Acta Met. 16, 1189 (1968).

137. C. K. Hari Dharan, "The Dynamic Behavior of Aluminum at High Strain Rates," Ph.D. Thesis, University of California, Berkeley, Oct. 1968.

138. M. P. Victoria, C. K. H. Dharan, F. E. Hauser and J. E. Dorn, J. Appl. Phys. 41, 674 (1970).

139. S. J. Green, C. J. Maiden, S. G. Babcock and F. L. Schierloh, "The High Strain-Rate Behavior of Face Centered Cubic Metals, Proceeding of the Battelle Colloquium on Inelastic Behavior of Solids, Columbus and Atwood Lake, Ohio, Sept. 1969.

140. A. Kumar and R. G. Kumble, J. Appl. Phys. 40, 3475 (1969).

141. J. W. Edington, Phil. Mag., June, 1189 (1969).

142. A. K. Mukherjee, W. G. Ferguson, W. L. Barmore and J. E. Dorn, J. Appl. Phys. 37, 3707 (1966).

143. T. L. Larsen, S. L. Rajnak, F. E. Hauser and J. E. Dorn, J. Mech. Phys. Solids, 12, 361 (1964).

144. W. G. Ferguson, F. E. Hauser and J. E. Dorn, Brit. J. Appl. Phys. 18, 411 (1967).

145. S. Yoshida and N. Nagata, Trans. Japan Inst. Metals 9, 110 (1968).

146. J. D. Campbell and W. G. Ferguson, Phil. Mag. 21, 63 (1970).